

Crystal Structure of Group II Chaperonin in the Open State

Yanwu Huo,^{1,7} Zhongjun Hu,^{1,2,7} Kai Zhang,^{1,7} Li Wang,³ Yujia Zhai,¹ Qiangjun Zhou,¹ Gabe Lander,⁴ Jiang Zhu,⁵ Yongzhi He,³ Xiaoyun Pang,¹ Wei Xu,¹ Mark Bartlam,⁶ Zhiyang Dong,^{3,*} and Fei Sun^{1,*}

¹National Laboratory of Biomacromolecules, Institute of Biophysics (IBP), Chinese Academy of Sciences, Beijing 100101, China

²Department of Physics, Logistics Engineering University, Chongqing 401311, China

³The State Key Laboratory of Microbial Resources, Institute of Microbiology, Chinese Academy of Sciences, Beijing 100101, China

⁴The Scripps Research Institute, 10550 North Torrey Pines Road, La Jolla, CA 92037, USA

⁵Vaccine Research Center, National Institute of Allergy and Infectious Diseases, National Institutes of Health, 40 Convent Drive, Bethesda, MD 20892-3027, USA

⁶College of Life Sciences, Nankai University, Tianjin, China

⁷These authors contributed equally to this work

*Correspondence: dongzy@sun.im.ac.cn (Z.D.), feisun@ibp.ac.cn (F.S.)

DOI 10.1016/j.str.2010.07.009

SUMMARY

Thermosomes are group II chaperonins responsible for protein refolding in an ATP-dependent manner. Little is known regarding the conformational changes of thermosomes during their functional cycle due to a lack of high-resolution structure in the open state. Here, we report the first complete crystal structure of thermosome (rATcpn β) in the open state from *Acidianus tengchongensis*. There is a $\sim 30^\circ$ rotation of the apical and lid domains compared with the previous closed structure. Besides, the structure reveals a conspicuous hydrophobic patch in the lid domain, and residues locating in this patch are conserved across species. Both the closed and open forms of rATcpn β were also reconstructed by electron microscopy (EM). Structural fitting revealed the detailed conformational change from the open to the closed state. Structural comparison as well as protease K digestion indicated only ATP binding without hydrolysis does not induce chamber closure of thermosome.

INTRODUCTION

Chaperonins are a class of molecular chaperones (Hemmingsen et al., 1988), oligomeric complexes that act as protein folding cages and facilitate proper protein folding through ATP consumption. Chaperonins have been classified into two subfamilies (group I and group II) based on their structure and sequence (Kim et al., 1994). Group I chaperonins exist in bacteria, mitochondria, and chloroplasts, as exemplified by the well-studied *Escherichia coli* chaperonin GroEL (Bukau and Horwich, 1998; Ranson et al., 2006). Group II chaperonins are found in archaea (Phipps et al., 1991) or eukaryotic cytosol (Frydman et al., 1992; Gao et al., 1992). Archaeal group II chaperonins are also referred as thermosomes due to their extreme thermal stability (Bigotti and Clarke, 2008). In eukaryotes, the cytosolic

group II chaperonin containing TCP-1 (CCT) is reported to facilitate the correct folding of cellular cytoskeletal elements such as actin and tubulin (Gao et al., 1992; Yaffe et al., 1992).

A common feature shared by group I and II chaperonins is a characteristic double ring structure, in which each subunit contains three domains: an equatorial domain that contains an ATP-binding site and is involved in interring contacts, an apical domain for substrate binding, and an intermediate domain that connects the equatorial and apical domains via flexible hinges (Ditzel et al., 1998; Xu et al., 1997). One of the major differences between these two groups is that group I requires the cofactor GroES (Tilly et al., 1981) to form a single ring and enclose the cage, whereas group II has a covalently attached lid domain that extends from the apical domain to cover the cage (Ditzel et al., 1998). Another difference is that whereas a group I chaperonin always consists of two homoheptameric rings (Xu et al., 1997), each ring of a group II chaperonin consists of eight or nine hetero- or homosubunits (Ditzel et al., 1998; Frydman et al., 1992; Schoehn et al., 2000; Shomura et al., 2004; Xu et al., 1997).

Before this work, two available crystal structures of thermosomes from both *Thermoplasma acidophilum* (Ditzel et al., 1998) and *Thermococcus* sp. strain KS-1 (Shomura et al., 2004) were shown to adopt a tightly closed conformation, exhibiting apical domains and interring contacts that differ from group I chaperonins. However, various conformations of group II chaperonins were described by cryoEM reconstruction, including closed forms, open forms, and asymmetric bullet-shaped forms, indicating the existence of domain movement during their functional cycles (Clare et al., 2008; Schoehn et al., 2000). In the absence of nucleotides, both thermosomes and CCT were found to have an open form (Llorca et al., 1999; Nitsch et al., 1998). Furthermore, the open and closed states of CCT have recently been comparatively modeled based on middle resolution cryoEM maps, suggesting that the lid closure was achieved by $\sim 25^\circ$ rotation of the intermediate domain and additional 50° rotation of the apical domain toward the equatorial domain (Booth et al., 2008). However, comparison between 8 Å cryoEM structure of thermosome Mm-cpn in the open state and its 4.3 Å cryoEM structure in the closed state suggested the chamber closure was completed by the inward movement of the entire

subunit (Zhang et al., 2010). As a result, the detailed conformational changes during transition from open to close is still not well characterized due to the lack of a high-resolution structure for group II chaperonin in open state. Furthermore, the substrate binding determinants are unclear for group II chaperonins. Besides, there are two models describing the transition from the open to closed state. One model suggests that the binding of ATP triggers chamber closure (Iizuka et al., 2003), while the other model suggests that it is the ATP hydrolysis that induces the closed conformation (Bigotti and Clarke, 2008). Those questions are importantly related to understand the molecular function of group II chaperonin and need to be carefully investigated.

The archaea *Acidianus tengchongensis* strain S5 grows in the Tengchong acidothermal springs in Southwestern China with an optimal temperature of 70°C and pH of 2.5. Two genes of this archaea (*cpn α* and *cpn β*) were found to encode two types of chaperonin subunits (ATCpn α and ATCpn β) that can assemble into thermosomes either homogeneously or heterogeneously (Wang et al., 2010). Preliminary studies have shown that recombinant ATCpn α (rATCpn α) assembles into an 8-fold double ring structure, recombinant ATCpn β (rATCpn β) into a 9-fold structure, and a combination of rATCpn α and rATCpn β assembles into a 9-fold heterooligomer with 1:2 stoichiometry (Wang et al., 2010). Both heterooligomer and homooligomer show trace ATP hydrolysis activity and limited refolding activity in vitro (Wang et al., 2010).

In this study, we focus on describing the 9-fold structures of rATCpn β by X-ray crystallography and electron microscopy. We solved the first high-resolution (3.7 Å) structure of complete group II chaperonin in its open state and found that its conformational changes from the open to closed state are achieved by both ~30° intrinsic rotation of lid and apical domains and the inward movement of the entire subunit. The conspicuous hydrophobic patch in the lid domain was found conserved across species and believed as a potential substrate-binding site. Structural analysis and protease K digestion assay suggested only ATP binding without hydrolysis could not trigger a closed structure for group II chaperonin.

RESULTS AND DISCUSSION

Crystal Structure of rATCpn β in the Open State

The protein rATCpn β was cloned, heterogeneously expressed in *E. coli* and purified by chromatography. Purified rATCpn β was assembled into thermosomes in vitro under proper conditions (see Experimental Procedures). The rATCpn β thermosome complexes (if not indicated, rATCpn β will be used to represent the rATCpn β thermosome discussed below) were successfully crystallized into two different crystal forms (Form I and Form II). Both Form I and Form II share the same C2 space group, although Form I crystals have a larger unit cell than Form II (Table 1). Using the Matthews coefficient estimation, 27 rATCpn β monomers (one and a half of rATCpn β thermosomes) were calculated to occupy the asymmetrical unit of Form I, and nine monomers (half of a rATCpn β thermosome) of Form II. The crystal structures of Form I and Form II were determined by molecular replacement using a model built from the cryoEM map of rATCpn β and were finally refined to 3.8 Å (Rwork 36.5% and Rfree 37.1%) for Form I and to 3.7 Å (Rwork 27.7% and Rfree

Table 1. Table X-Ray Diffraction Data Collection and Refinement Statistics

Data Collection	Form I	Form II
Space group	C2	C2
Cell Dimensions		
a, b, c (Å)	501.0, 276.3, 161.0	223.7, 283.0, 160.8
alpha, beta, gamma (°)	90.00, 106.8, 90.00	90.0, 133.9, 90.0
Resolution (Å)	50.0–3.80 (3.94–3.80)	50.0–3.70 (3.90–3.70)
R _{merge} ^a	0.181 (0.390)	0.117 (0.476)
I/σ	9.0 (1.6)	7.4 (2.3)
Completeness (%)	97.0 (81.4)	99.5 (99.4)
Redundancy	3.2 (2.5)	3.2 (3.3)
Refinement		
Resolution (Å)	50.0–3.80	50.0–3.70
No. reflections	199,545	76,576
R _{work} /R _{free} (%) ^b	36.5/37.1	27.7/28.3
No. Atoms		
Protein (one subunit)	3849	3849
Ligand/ion (ADP)	—	27
B Factors (Å ²)		
Equator domain	70.4	108.5
Median domain	108.1	135.0
Apical domain	112.0	137.2
Lid domain	118.8	147.1
Rmsds		
Bond lengths (Å)	0.01	0.01
Bond angles (°)	1.41	1.48

Corresponding parameters for the highest resolution shell are shown in parentheses.

^a R_{merge} = $\sum_h \sum_i |I_{ih} - \langle I_h \rangle| / \sum_h \sum_i \langle I_h \rangle$, where $\langle I_h \rangle$ is the mean intensity of the observation I_{ih} reflection h .

^b R_{work} = $\sum (||F_p(\text{obs})| - |F_p(\text{calc})||) / \sum |F_p(\text{obs})|$; R_{free} = R factor for a selected subset (5%) of the reflections that was not included in prior refinement calculations.

28.3%) for Form II. The statistics of data collection and structural refinements are summarized in Table 1. Although the structure determined in Form I is similar to that of Form II, the better diffraction data quality of Form II resulted in a more precise map (see Figure S1 available online). For this reason, only the Form II crystal structure was used for further analysis.

Of the 553 residues present in each rATCpn β subunit, residues 1–27 and 533–553 were not assigned due to the lack of electron density. The rATCpn β subunit itself shares a common fold with other group II chaperonins, consisting of an equatorial (residues 28–149 and 412–532), intermediate (residues 150–224 and 377–411), apical (residues 225–252 and 283–376), and lid domain (residues 253,282) (Figures 1A and 1B). The equatorial domain contains a seven-helix bundle (H1–H4–H12–H13 and H3–H5–H16) flanked by three helices (H2, H14, and H15) and five β strands (S1, S2, S15, S16, and S17). The β strands S1 and S2 form a β sheet by interacting with the strand S17 from the adjacent subunit. The intermediate domain is mainly made up of a three-helix bundle (H6, H7 and H11) next to a two stranded β sheet (S4 and S14). The apical domain contains

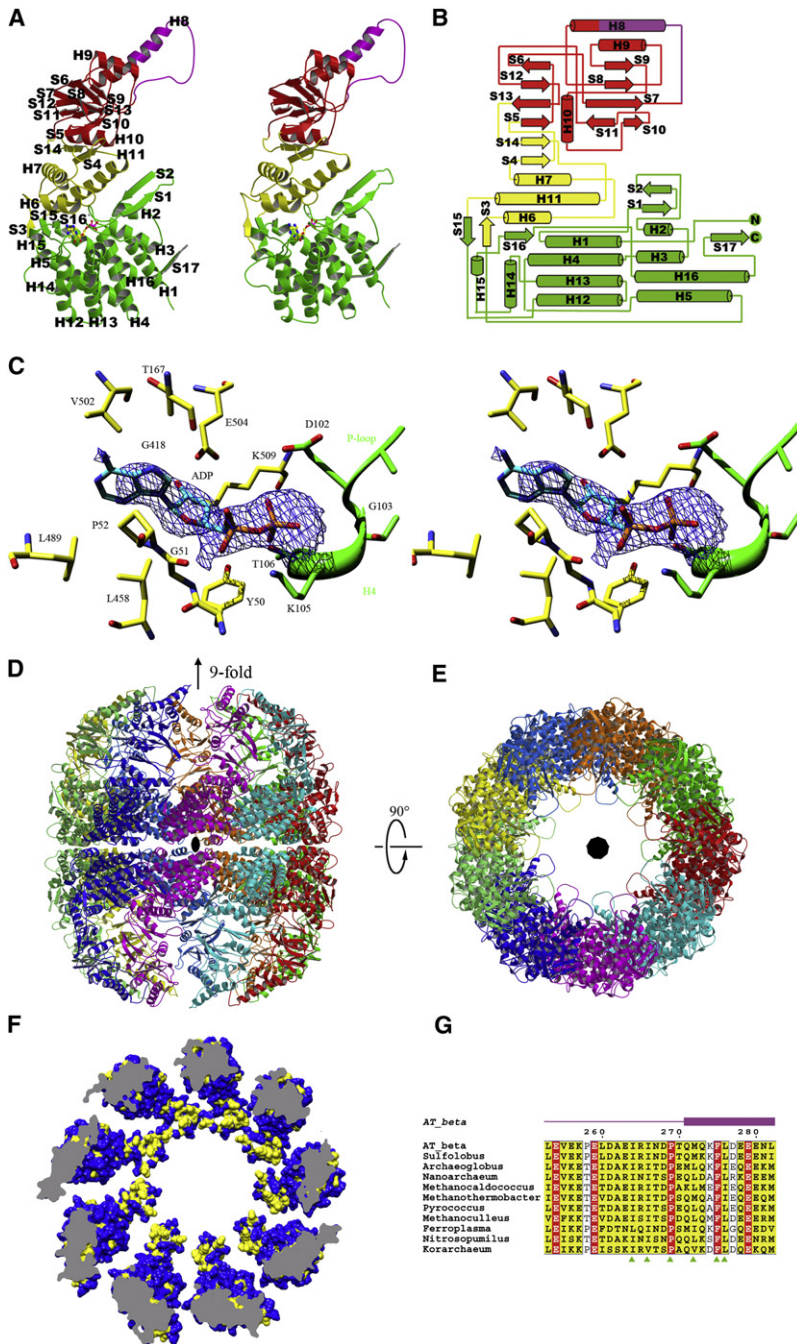


Figure 1. Crystal Structure of rATcpnβ

(A) Structural features of the rATcpnβ monomer, colored by domain. The lid is purple, apical domain is red, intermediate domain is yellow, and the equatorial domain is green. The modeled ADP is colored by element.

(B) Topology of rATcpnβ monomer.

(C) The stereo view of nucleotide binding site of rATcpnβ.

The 2Fo-Fc omit difference map (contour level 0.8) shows an elongated stretch of electron density on top of the equatorial domain, into which the ADP could be modeled.

The adjacent residues involved in interaction are labeled.

(D and E) Side and top views of overall rATcpnβ structure.

(F) Hydrophobic patch in the lid domain of group II chaperonin. Hydrophobic surface representation of rATcpnβ crystal structure. The hydrophobic surface is colored by yellow and the hydrophilic by blue.

(G) Sequence alignments of thermosomes across several species reveal hydrophobic patch in the lid is conserved and corresponding site is indicated in green triangle. The GenBank accessions of protein sequences form top to bottom are AAO47380, YP_255343, YP_003400009, NP_963436, YP_003459021, NP_275933, NP_142040, YP_001048251, ZP_05570324, ABX13688, and ACB08055, respectively.

See also Figure S1.

crystallization buffer, the crystal structure of rATcpnβ exhibits an open conformation with 9-fold symmetry. Superposition of the rATcpnβ and TAcpnα/TAcpnβ/TKcpn subunits yields a large structural rmsd (root mean square deviation) of 1.4/1.7/2.4 Å for the 460/468/470 Cα atoms, respectively (Figure 2A), despite a high sequence homology (75% sequence similarity and 54% identity) (Figure S2). The individual domains (equatorial, intermediate, apical, and lid) of rATcpnβ and TKcpn were further compared by superposition, yielding rmsd values of 1.0/0.8/0.9/1.3 Å for the 217/93/115/25 Cα atoms, respectively. The high degree of structural similarity among the apical, intermediate, and equatorial domains demonstrates that these domains are not flexible. The high rmsd value of the lid domain is due to its inherent structural plasticity (Ditzel et al., 1998; Klumpp et al., 1997). The different structural conformations between the rATcpnβ and TKcpn monomers are due to domain rotation and flexibility of the lid domain (Movies S1 and S2). There is

two β sheets (S5-S6-S12-S13 and S7-S8-S9-S10-S11) surrounded by two α helices (H9 and H10) above and below. The protruding lid is mainly comprised of α helix H8 and a flexible loop between H8 and S7. The nucleotide binding site is located directly above the equatorial domain, as evidenced by a clear density in the omit 2FoFc map (Figure 1C).

In contrast to the thermosome crystal structures from *Thermoplasma acidophilum* (TAcpn) (Ditzel et al., 1998) and *Thermococcus sp.* strain KS-1 (TKcpn) (Shomura et al., 2004), both of which adopt a closed form with 8-fold symmetry which might be caused by high concentration of ammonium sulfate in the

a ~30° rotation of the apical and lid domain between rATcpnβ and TKcpn monomers (Figure 2A).

In Form II crystals, two asymmetric units make up the complete rATcpnβ thermosome, comprising two stacked, nine subunit rings correlated by the crystallographic 2-fold axis. The rATcpnβ thermosome adopts an open state that differs from all previously reported closed structures (Ditzel et al., 1998; Shomura et al., 2004), exhibiting an overall cylindrical shape with a height of 185 Å along the 9-fold axis and a diameter of 168 Å along the 2-fold axis (Figures 1D and 1E). Each subunit has a surface area of 25,600 Å². The intraring contacts between

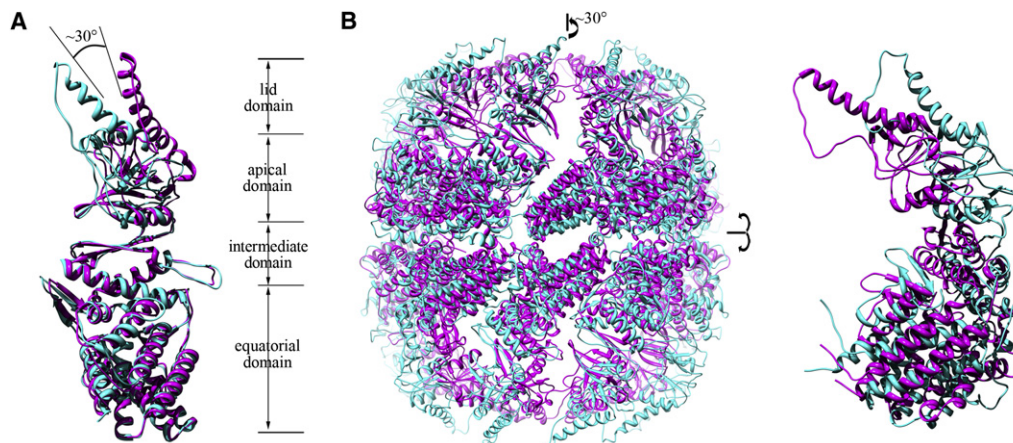


Figure 2. Comparison of the Monomer and Overall structures of the Two Thermosome States

(A) The rATcpn β crystal structure is an open state colored in cyan. The TKcpn crystal structure represents the closed state colored in pink. (B) Superposition of the overall structures for rATcpn β in the open state (cyan) and closed state (pink) based on the cryoEM and nsEM map, respectively. One isolated subunit is enlarged and shown on the right. See also Figure S2 and Movies S1–S5.

adjacent subunits are localized mainly at the equatorial domains through interactions mediated by β strands S1, S2, and S17, with a surface area of about 970 \AA^2 (Figures 1A and 1D). For interring interaction, each subunit interacts with only one subunit of the opposite ring through its equatorial domain. This interring contact interface is about 630 \AA^2 , with electrostatic interactions mediated by eight pairs of salt bridges.

Around the inner surface of the chamber, there is a conspicuous hydrophobic patch located in the lid domain, which is composed of residue Ala262, Ile264, Ile266, Pro269, Met272, Phe275, and Leu276 (Figures 1F and 1G). Based on the sequence alignment of thermosome among representative species, it was found that those residues are highly conserved with two invariant residues Pro269 and Phe275 across species (Figure 1G), suggesting those residues might be the substrate binding determinants.

Electron Microscopy Study of rATcpn β and Structural Fitting

We prepared the purified rATcpn β sample in the presence and absence of ATP (referred to below as rATcpn β _ATP or rATcpn β _apo, respectively) for cryoelectron microscopy (cryoEM) studies. Two-dimensional image analysis, intensive 2D classification and averaging of more than 40,000 rATcpn β _apo/rATcpn β _ATP particle images revealed many classes with top views of 9-fold symmetry and a small portion ($\sim 10\%$) of 10-fold symmetry (Figures 3A and 3B) that was confirmed by blue native PAGE (Figure S3). Three-dimensional cryoEM structures of rATcpn β _apo and rATcpn β _ATP with imposed 9-fold symmetry were reconstructed with resolution 8.8 and 8.4 \AA that were determined by RMEASURE, respectively (Sousa and Grigorieff, 2007). Both cryoEM structures share similar cylindrical shape with a diameter of 173 \AA and a height of 180 \AA and exhibit an open conformation with the bottom lid domain density missing (Figure 3C). Interestingly, the top lid domain density is clearer in rATcpn β _ATP than in rATcpn β _apo, which suggests the flexibility of lid domain is reduced after ATP binds

to thermosome. In accordance with the open crystal structure, the interring and intraring contacts in cryoEM maps are only involved in the equatorial domains and the intermediate and apical domains are disconnected.

Docking the thermosome TKcpn subunit structure (PDB 1Q3R) en bloc into the cryoEM map of rATcpn β _ATP does not yield good fit (Figure S4). The octadecamer model, built by fitting 18 TKcpn subunits into the cryoEM map, shows severely loose intraring interactions, invalidating such a model (Figure S5). Docking the crystal structure of the rATcpn β subunit into the same cryoEM density, all equatorial, intermediate, and apical domains exhibit an excellent fit. By observation, most structural elements (α helices, β sheets, and loops) fit the density tubes, layers, and blobs precisely (Figure 3D). Most importantly, the helical protrusion of the lid domain fits well into lid density of the upper ring (Figure 3D), indicating that the crystal structure of rATcpn β shares the same open state observed in the cryoEM map.

Although different conditions were tried many times, no rATcpn β structure in closed conformation could be found by cryoEM study at all. However, the rATcpn β thermosome examined by negative staining electron microscopy (nsEM) appears as a 9-fold closed structure (Figure 4). The relatively even orientation distribution enabled us to reconstruct the structure of rATcpn β to 14 \AA resolution that was assessed by RMEASURE (Sousa and Grigorieff, 2007). The overall nsEM structure exhibits an oblong sphere shape with a diameter of 170 \AA and a height of 160 \AA (Figure 4C). Its particularly salient feature is that both rings adopt a closed conformation.

The crystal structure of rATcpn β subunit could not fit into either the top or bottom ring of nsEM map very well (Figure S4). The octadecamer model built by fitting eighteen rATcpn β subunits into the nsEM map shows severe structural collisions around the lid domain, indicating that it is an incorrect model (Figure S5). Whereas, docking the subunit from the crystal structure of closed-state TKcpn thermosome into the nsEM map provides a fairly good fitness (Figure 4D). Due to the good fitness

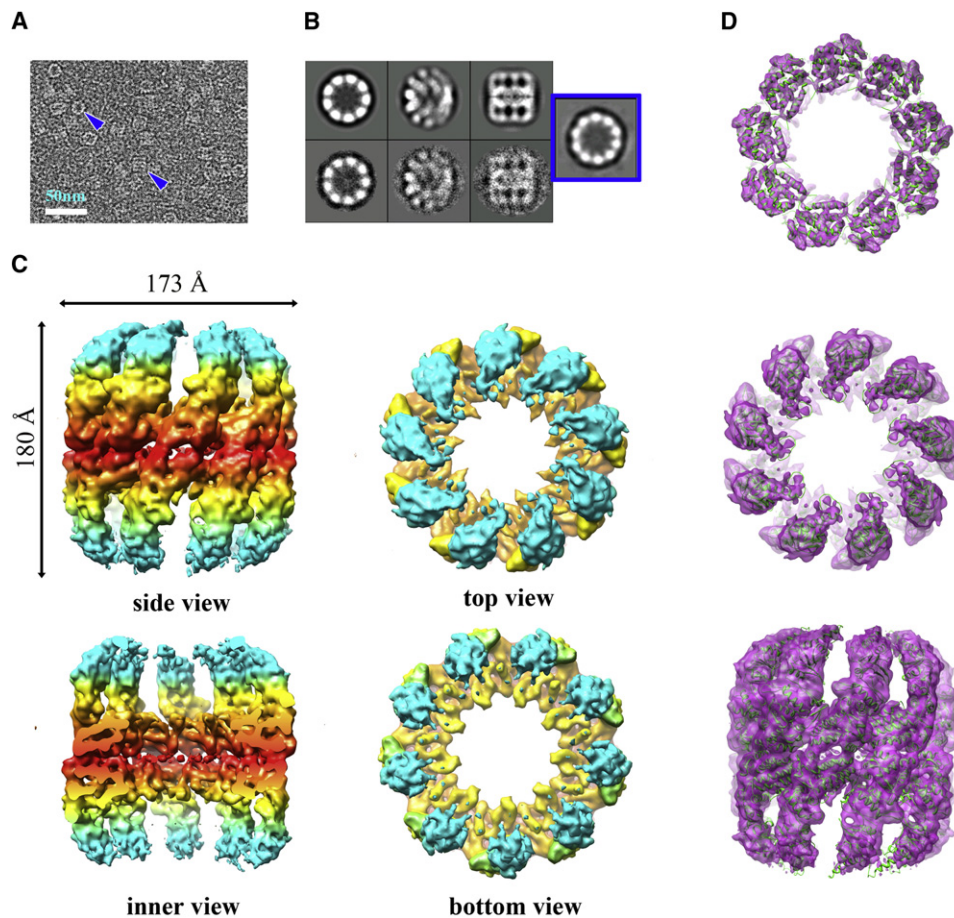


Figure 3. CryoEM Structure of rATcnp β in Open State and Atomic Structure Fitting

(A) Raw image of particles in cryo-EM. Top and side views are indicated by blue arrows. The scale bar is 50 nm.

(B) Averaging views (top, tilt, and side) of selected 2D classes of cryoEM particles of rATcnp β _ATP are matched to the corresponding 3D projections. The top view exhibiting 10-fold symmetry, with a small portion (~10%) from 2D classification indicated in the blue square.

(C) Surface representation of the side, inner, top, and bottom views of the cryo-EM structure of rATcnp β _ATP. The cryo-EM structure of rATcnp β _apo is similar to rATcnp β _ATP and not shown here. EM map are colored based on domain division, with the apical and lid domains in cyan, the intermediate domain in yellow, and the equatorial domain in red.

(D) Equatorial, apical, and side views of the rATcnp β subunit crystal structure fit into the rATcnp β _ATP cryo-EM map.

See also Figures S3–S5.

and low resolution of nsEM map, the fitted model was not further optimized by flexible modeling tools. The structural fitting indicates that the nsEM structure of rATcnp β shares the same closed conformation with the closed structure of TKcnp but not the open structure of rATcnp β .

Implication Based on Structural Comparison and Analysis

It might be considered whether the subunit conformational difference between the rATcnp β open structure and the TKcnp closed structure is derived from their different symmetries. The conclusion is negative since the 8-fold structure of rATcnp α was also successfully reconstructed by cryoEM and shows an open conformation (K.Z., L.W., and F.S., unpublished data), which could be fitted better by the crystal structure of rATcnp β than by the TKcnp structure. As a result, sharing with very high-sequence homology, such large conformational difference

between rATcnp β and TKcnp should have their biological significance.

All of above, it is clear that either cryoEM structures or crystal structure of rATcnp β depict the similar open conformation, while the nsEM structure of rATcnp β has a closed conformation. Supposing these two different conformations represent their biological states, it is necessary to compare them further and investigate the conformational change during transition from open to closed state. The rATcnp β thermosome models in open and closed form were aligned after superimposing their 9-fold axes and equatorial planes, exhibiting large conformational changes (Figure 2B). Both a $\sim 30^\circ$ counterclockwise rotation of the apical and lid domains and an inward movement of the entire subunit were found to be indispensable for transition from the open to the closed state (Movies S3–S5), which fixed the previous confused reports that lid closure of CCT needs domain rotation (Booth et al., 2008), but the closing chamber of thermosome

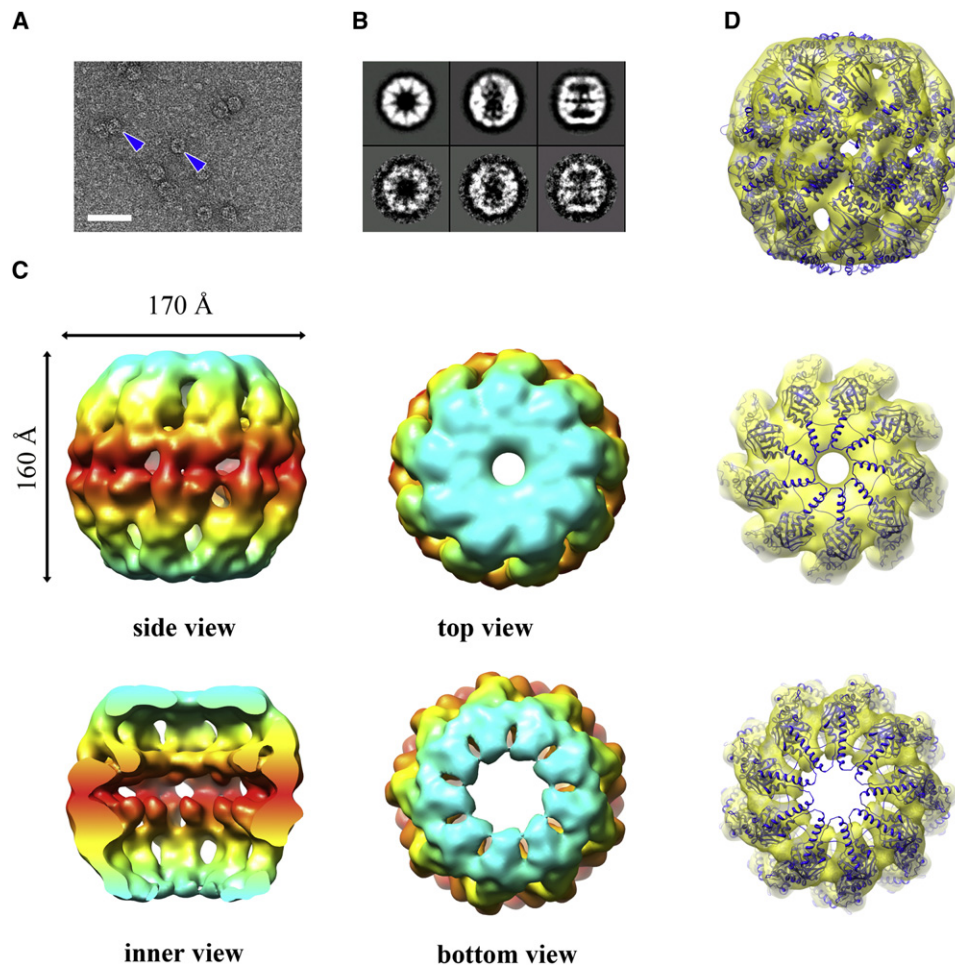


Figure 4. Negative Staining EM Structure of rATcpn β in Closed State and Atomic Structure Fitting

(A) Raw EM image of negatively stained particles. Top and side views are indicated by blue arrows. The scale bar is 50 nm.

(B) Averaging views (top, tilt, and side) of selected 2D classes of the negatively stained particles are matched to the corresponded 3D projections.

(C) Surface representation of the side, inner, top, and bottom views of the negative stain structure. EM map are colored based on domain division, with the apical and lid domains in cyan, the intermediate domain in yellow, and the equatorial domain in red.

(D) Side, top, and bottom views of the TKcpn subunit crystal structure fit into the rATcpn β nsEM map.

See also Figures S4–S5.

Mm-cpn requires the inward movement of entire subunit (Zhang et al., 2010). In addition, only the rotation of the lid and apical domains was observed for rATcpn β and there is no rotation for intermediate domain with respect to equatorial domain, which is different to the medium-resolution cryoEM study of CCT (Booth et al., 2008). Upon the high-resolution structure of rATcpn β in open state, the detailed conformational changes described in this work are much clearer and more accurate than before. Furthermore, such kind of conclusion was even strengthened when we compared the open cryoEM model of 8-fold rATcpn α with the crystal structure of closed TKcpn thermosome and found the exact same conformational changes (K.Z., L.W., F.S., unpublished data).

What kinds of biological states do the open structures of rATcpn β represent? The 2FoFc omit map in the crystal structure of rATcpn β indicates it is a nucleotide-binding structure (Figure 1C). The nucleotide was further analyzed by high-perfor-

mance liquid chromatography experiments and recognized as ADP. Comparison between the cryoEM maps of rATcpn β _apo and rATcpn β _ATP showed clear additional density at the nucleotide-binding site in rATcpn β _ATP (Figure 5A), which confirmed that the open structures of rATcpn β _ATP and rATcpn β _apo represent the ATP-binding state and nucleotide-free state, respectively. As a result, it is clear that nucleotide binding would not trigger the nucleotide-free structure of rATcpn β from the open state to the closed state, which was further proved by protease K digestion experiments. In the presence of different nucleotides (ATP or ADP), the rATcpn β thermosome exhibits sensitivity to protease K digestion (Figure 5B), indicating it keeps the open conformation with or without nucleotide binding because it was reported that the closed thermosome was resistant to cleavage by protease (Iizuka et al., 2003). The fact that ATP binding does not induce a closed structure of rATcpn β is different from Mm-cpn and CCT (Booth et al., 2008; Zhang

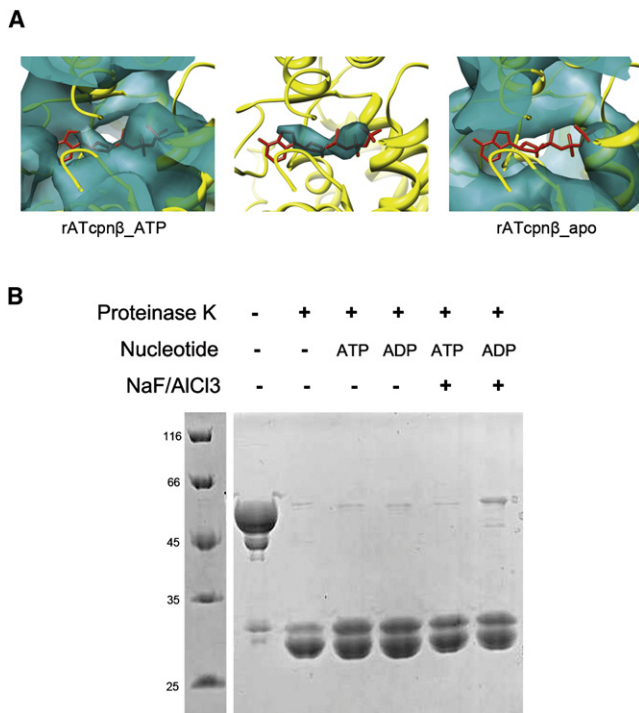


Figure 5. ATP Binding without Hydrolysis Could Not Trigger a Closed Structure for Group II Chaperonin

(A) A comparison of the electron density near the ATP-binding sites of the rATcpnβ_{apo} and rATcpnβ_{ATP} cryoEM maps. On the left the rATcpnβ crystal structure is fitted into the rATcpnβ_{ATP} cryoEM map. The middle shows the difference map between the rATcpnβ_{ATP} cryoEM map and the rATcpnβ crystal structure with ADP omitted. The right shows the rATcpnβ crystal structure is placed into the rATcpnβ_{apo} cryoEM map. ATP shown as red stick model is placed into the nucleotide binding pocket.

(B) Protease K digestion assay of rATcpnβ under different conditions. The rATcpnβ incubated with ADP, ATP, ADP/NaF/AIF₃, or ATP/NaF/AIF₃ were digested by protease K at 65°C for 5 min. Each lane is labeled.

et al., 2010). We further conclude that it is not due to the temperature because the protease K digestion experiment was carried at physiological temperature. Meanwhile, we incubated rATcpnβ thermosome in its physiological temperature with the presence of ATP and AIF₃ before rapid freezing and did not find the closed structure by the subsequent cryoEM study. We speculate that it is the low ATP hydrolysis activity of rATcpnβ (Wang et al., 2010) to keep ATP bound to rATcpnβ without hydrolysis and enable us to observe the authentic open structure of rATcpnβ in ATP bound state. In contrast, when Mm-cpn thermosome or CCT was mixed with ATP and AIF₃, ATP would be hydrolyzed into ADP and the ATP hydrolysis transition state could be only captured. As a result, our structural study would further support the opinion that only ATP binding without hydrolysis could not drive the conformation from the open to the closed state for group II chaperonin.

Conclusions

Before this work, without a high-resolution structure of group II chaperonin in the open state, researchers could only separate the closed crystal structure into equatorial, intermediate, and

apical domains and fit the individual domains into the open-state cryoEM map to obtain a pseudo atomic model of group II chaperonin in the open state (Booth et al., 2008; Clare et al., 2008). Here, we presented the first high-resolution (3.7 Å) complete structure of group II chaperonin in the open state which could be fit into the open state cryoEM map perfectly so that the conformational changes from the open to the closed state could be precisely described in details. In our study, it is found that the detailed conformational changes during transition from the open to the closed state could be achieved by ~30° intrinsic rotation of lid and apical domains and the inward movement of entire subunit. Either domain rotation or subunit movement alone could not complete the chamber closure of group II chaperonin. Furthermore, the conspicuous hydrophobic patch in the lid domain was found conserved across species and might be a potential substrate-binding site that needs to be further investigated. Structural analysis and protease K digestion assay suggested only ATP binding without hydrolysis could not trigger a closed structure of group II chaperonin.

EXPERIMENTAL PROCEDURES

Molecular Cloning of rATcpnβ

The molecular cloning of rATcpnβ was performed as recently reported (Wang et al., 2010). In brief, genomic DNA of *Acidianus tengchongensis* strain S5 was prepared as described by Lauerer et al. (1986). The complete sequence of rATcpnβ gene was measured by inverse PCR (Ochman et al., 1988). The cDNA of rATcpnβ was amplified by PCR taken the genomic DNA as template and then subcloned into pET23b within NdeI and BamHI restriction sites.

Expression and Purification of rATcpnβ

The rATcpnβ protein was overexpressed in the *E. coli* strain Rosetta-gamiTM B(DE3)pLysS (Novagen) using the pET23b expression vector (Novagen). The recombinant bacteria were grown in Terrific Broth medium (TB) at 37°C. When the optical density (OD) of the culture at 600 nm reached 1.6~1.8, isopropyl β-D-1-thiogalactopyranoside (IPTG) was added to a final concentration of 0.4 mM. The culture was further incubated for 20 hr at 16°C. The harvested cells were broken in buffer A (20 mM Tris-HCl, pH 8.0, 5 mM EDTA-Na, 5 mM MgCl₂) by sonication. After centrifugation for 20 min at 10,000 × g, the supernatant was incubated at 80°C for 30 min. After further centrifugation for 20 min at 10,000 × g, the supernatant was applied to the Q-Sepharose fast flow column (GE Healthcare) that was preequilibrated by buffer A. After washing, the column was eluted using a linear NaCl gradient from 0 to 0.6 M in buffer A. The target rATcpnβ protein was eluted at 0.14 M NaCl, fractionated, and dialyzed against buffer A overnight at 4°C. After dialysis, the protein was treated with 0.25 mM ATP and 1 M (NH₄)₂SO₄ at 37°C for 5 hr to facilitate rATcpnβ assembly and then concentrated using an Amicon Ultra-15 filter (Millipore). The concentrated solution was applied to the Superdex 200 10/300 GL column (GE Healthcare), and the fully assembled rATcpnβ thermosomes were eluted using buffer A, separate from the monomers. The fractions were collected, concentrated to ~20 mg/ml and stored at -80°C. The purity of rATcpnβ was analyzed by SDS-PAGE and blue native PAGE.

Blue Native PAGE

The concentration of the sample gel was 4% and the gradient separation gel concentration ranged from 5% to 13%. The loading amount of sample was about 100 μg. Blue native PAGE (BN-PAGE) was performed at 4°C in a vertical apparatus with a deep blue cathode buffer B (50 mM Tricine, 7.5 mM imidazole [pH 7.0], 0.02% Coomassie blue G-250). At the beginning of the gel running, the electrophoresis voltage was maintained at 100 V until the sample entered into the sample gel. Then, the electrophoresis current was kept as a constant 15 mA, and the electrophoresis voltage was limited to below 500 V. After about one-third of the total running distance, the cathode buffer B was replaced by cathode buffer B/10 for overnight electrophoresis (Wittig et al., 2006). After running BN-PAGE the gel was stained by Coomassie blue R250.

Electron Microscopy, Image Processing, and 3D Reconstruction

For negative staining electron microscopy, 5 μl of 1 mg/ml rATcpn β was applied to a glow-discharged carbon-coated grid that was stained with 5 μl of 2% uranyl acetate. The negative stained rATcpn β was imaged on a transmission electron microscope Tecnai T20 (FEI, Netherlands) with a LaB₆ electron source, operated at 200 kV. The electron micrographs were recorded on a 2Kx2K UltraScan 894 CCD camera (Gatan) with a nominal magnification of 70,000 and a pixel size of 2 \AA . The contrast transfer function (CTF) of each CCD image was determined using CTFIND3 (Mindell and Grigorieff, 2003) and corrected by phase flip using CTFINDA from the Image2000 package (Crowther et al., 1996). After manual particle selection, ~2300 selected particles were classified and averaged using the program “refine2d.py” in the EMAN suite (Ludtke et al., 1999). A 3D initial model was created using the program “startcsym” and further refined using “refine” from the EMAN suite (Ludtke et al., 1999).

For cryoelectron microscopy, either 2 μl of rATcpn β (the purified rATcpn β monomers were assembled into thermosomes with existence of ATP so this sample was placed in refrigerator for two weeks to make ATP fully hydrolyzed and released before plunge freezing) at 20 mg/ml or 3 μl of rATcpn β -ATP-ALF₃ at 12 mg/ml was applied to a C-flat grid (r/2/2, Protochips Inc.) and treated by the Solarus plasma cleaner system (Model 950, Gatan). The grids were then blotted and plunged into liquid ethane using a Vitrobot (FEI, Netherlands) running at 4°C and 95% humidity, transferred to a CT3500 cryo-holder (Gatan) and loaded into a Tecnai F20 FEG electron microscope (FEI, Netherlands). The electron microscope was operated at 120 kV and the rATcpn β -apo and rATcpn β -ATP samples were imaged using the LEGION (Carragher et al., 2000; Suloway et al., 2005) automatic data acquisition system in the low-dose mode. The images were recorded on a 4Kx4K UltraScan 895 CCD camera (Gatan) with a final pixel size of 1.55 \AA .

Tens of thousands of particles were automatically selected using FindEM (Roseman, 2004). The CTF of each micrograph was determined using CTFIND3 (Mindell and Grigorieff, 2003) in the image2000 package (Crowther et al., 1996), and then the phases of each particle were corrected by using the “aplyctf” program in the EMAN suite (Ludtke et al., 1999). After two-dimensional classification and averaging by the program “refine2d.py” in the EMAN suite, several bad classes with no clear structural information were discarded. The initial model was created using the program “startcsym” in EMAN. Three Gaussian noises under the same level were added into the initial model, resulting in three starting models, which were further refined by using “multi-refine” in EMAN suite to remove the bad particles. Final refinements were performed using “refine” in EMAN with Spider scripts (Frank et al., 1996; Shaikh et al., 2008) embedded for correspondence analysis (CORAN) of each image class, wrapped in the Appion package (Lander et al., 2009). The final reconstructed density map was further sharpened by an amplitude correction algorithm using the program EM-BFACTOR (Fernandez et al., 2008). In summary, the rATcpn β -apo reconstruction used ~46,000 particles in the final refinement, and, for rATcpn β -ATP, ~69,000 particles were used.

The resolutions of the above 3D reconstructions were assessed by the program RMEASURE (Sousa and Grigorieff, 2007) using the FSC 0.143 threshold. In addition, the suggested resolutions of the nsEM map of rATcpn β , cryoEM map of rATcpn β -apo and the cryoEM map of rATcpn β -ATP are approximately 14, 8.8, and 8.4 \AA , respectively.

Crystallization of the rATcpn β and Postcrystal Treatment

It should be mentioned that purified rATcpn β monomers were assembled into thermosomes in vitro with existence of ATP so the sample used for crystallization contained ATP that was gradually hydrolyzed by rATcpn β for 1 week. Purified rATcpn β thermosome (6 mg/ml) was crystallized in 100 mM Tris-HCl, 1.2 M Li₂SO₄ (pH 8.0). Initially, leaf-shaped crystals were obtained with very weak diffraction. We optimized these rATcpn β crystals by mixing 1 μl of protein solution (5 mg/ml rATcpn β , 20 mM Tris-HCl [pH 8.0], 5 mM EDTA-Na, 5 mM MgCl₂) and 1 μl of mother liquid (100 mM Tris-HCl [pH 8.5], 1.0 M Li₂SO₄) at 289 K over a 200 μl reservoir solution (100 mM Tris-HCl [pH 8.5], 1.15 M Li₂SO₄) by the hanging drop vapor diffusion method. Some single crystals reached a size of 0.2 \times 0.2 \times 0.5 mm³. The diffraction of the rATcpn β crystals was dramatically improved by soaking them into a dehydration solution of 3.5 M ammonium sulfate for approximately 12 hr. Certain single, large crystals treated by dehydration could diffract to 6.0–4.5 \AA in-house, and then to

4.0~3.5 \AA in synchrotron radiation. After dehydration, the crystals were rapidly frozen in liquid nitrogen and stored for screening and data collection.

Data Collection and Processing

Diffraction data for the rATcpn β crystal Form I were collected on a beamline BL-5A (detector Quantum 315 CCD) of the Photon Factory (Tsukuba, Japan) at a temperature of 100 K and using radiation of wavelength 1.000 \AA . Because of the large unit cell and the poorly diffracting, highly mosaic crystal, the data collection parameters were carefully selected and controlled. In particular, the crystal-to-detector distance was set to 530 mm and the oscillation angle was set to 0.3° for diffraction overlap minimization. The exposure time was optimized to 10 s to balance the diffraction resolution and radiation damage.

One year later, a diffraction data set for rATcpn β crystal Form II was collected on the beam line BL-17A (detector Quantum 270 CCD) of the Photon Factory (Tsukuba, Japan) at a temperature of 100 K and using radiation of wavelength 0.900 \AA . The crystal-to-detector distance was set to 511.9 mm and the oscillation angle was set to 0.5°. The exposure time was optimized and set to 15 s.

The diffraction data sets were indexed, merged, and scaled using the HKL2000 program suite (Otwinowski and Minor, 1997) for crystal Form I and MOSFLM (Powell, 1999) for Form II; the data processing statistics are summarized in Table 1.

Molecular Replacement and Structural Refinement

Before diffraction data for crystal Form II were collected, the diffraction data set of Form I was used to determine the crystal structure by molecular replacement. Fitting the complete coordinates of the subunits from the TAcnp α , TAcnp β , or TKcpn thermosomes into the cryoEM map of rATcpn β did not yield a successful molecular replacement model. The correct starting model was manually built by fitting nine equatorial domains from the TKcpn subunits (pdb code: 1Q3R) into the cryoEM map of rATcpn β -apo using UCSF Chimera (Goddard, 2007), which resulted in a single ring model. This model was used for molecular replacement with Phaser (McCoy et al., 2007), which produced several equivalent and significant solutions. The solution with the highest translational likelihood gain (6531), Z-score (36.4), and good crystal packing was selected for further phasing.

Initial phasing yielded a clear electron density map around the equatorial domains, but a very poor and indiscriminate density around the other regions. The electron density map was dramatically improved by imposing the non-crystallographic symmetry (NCS) averaging technique, combined with phase extension from 10 to 3.8 \AA and a small extension step of ~0.002 \AA^{-1} in the reciprocal space. The averaged density map showed very good connectivity, and the secondary structures could be easily recognized. An initial polyaniline model was built manually using Coot (Emsley and Cowtan, 2004) under the guidance of the averaged map and topology of the TKcpn subunit. After rigid body refinement of the polyaniline model by Refmac5 (Winn et al., 2001), another round of NCS averaging and phase extension was applied to produce further improved electron density, from which large residues such as Trp and Tyr could be distinguished. These residues were assigned and used as reference points in the sequence to locate other residues. Refinements (rigid body, simulated annealing, energy minimization and group B factor) of the manually built model were performed with CNS (Brunger et al., 1998; Brunger, 2007) using a NCS restriction among the 27 subunits in one asymmetric unit. A negative B factor (DeLaBarre and Brunger, 2006) (–100 \AA^2) was applied to sharpen the 2Fo-Fc map, which was further used to rebuild the model and correct some errors. The final structure of rATcpn β in crystal Form I was refined to 3.8 \AA with an Rwork of 36.5%, Rfree of 37.1%, and an overall figure of merit (FOM) of 0.66.

The crystal structure of rATcpn β in Form II was solved by molecular replacement using the model from Form I. After several rounds of refinements, B factor sharpening with a negative B factor (DeLaBarre and Brunger, 2006) of –70 \AA^2 was applied to improve the electron density map, which was further used to correct some residues. The structure of rATcpn β in Form II was finally refined to 3.7 \AA with Rwork of 27.7%, Rfree of 28.3%, and an overall figure of merit (FOM) of 0.78. The stereochemistry of the final model was checked using the program PROCHECK (Morris et al., 1992) with the result that 80.9% (369) of the residues are in most favored regions, 17.8% (81) are in allowed

regions and 1.3% (6) are in generously allowed regions. The statistics for the structural refinements are summarized in Table 1.

Protease K Digestion Assay

The assay buffer was 50 mM Tris-HCl [pH 7.4], 100 mM KCl, and 25 mM MgCl₂. Chaperonins (0.35 mg/ml) were incubated without or with ADP (1 mM), ATP (1 mM), ADP (1 mM)/NaF (30 mM)/AlCl₃ (5 mM), ATP (1 mM)/NaF (30 mM)/AlCl₃ (5 mM), respectively, for 20 min at 75°C. Then digestion with protease K (20 ng/μl) was performed at 65°C for 5 min. Then PMSF (phenylmethylsulfonyl fluoride) was added into the mixture with final concentration 5 mM to inhibit the digestion of protease K before the sample was analyzed on 12.5% SDS-PAGE. Gels were stained with Coomassie brilliant blue.

Structural Analysis and Illustration

All structural superposition calculations were performed using the “align” command in PyMol (DeLano, 2002). The solvent accessible surface areas and interface areas of the thermosome subunits were calculated by the program PISA (Krissinel and Henrick, 2007). The EM maps were segmented, displayed, and fitted with crystal structures using UCSF Chimera (Pettersen et al., 2004).

All structural figures were generated by UCSF Chimera (Pettersen et al., 2004), Molscrip (Kraulis, 1991), Bobscrip (Esnouf, 1997), and PyMol (DeLano, 2002) as indicated.

ACCESSION NUMBERS

The rATcpnβ negative staining electron microscopy density map and the rATcpnβ_{apo} and rATcpnβ_{ATP} cryoelectron microscopy density maps were deposited in Electron Microscopy Data Bank (EMDB) with the access number EMD-5154, EMD-5159, and EMD-5157, respectively. The rATcpnβ_{ADP} crystal structure coordinates were deposited in the Protein Data Bank (PDB) with accession number 3KO1.

SUPPLEMENTAL INFORMATION

Supplemental Information includes five figures and five movies and can be found with this article online at doi:10.1016/j.str.2010.07.009.

ACKNOWLEDGMENTS

We thank Lingpeng Cheng (Institute of Biophysics, Chinese Academy of Sciences) for his help with UCSF Chimera and Ruigang Su (F.S. group) for his help preparing carbon-coated grids. We also thank Xudong Zhao, Ruimin Zheng, and Su liu (Core Facilities for Protein Sciences, CAS) for their help on maintaining the instruments of F.S.'s lab. This work was supported by NSFC grant (30770496, 30721003), “973” project (2006CB806506, 2006CB911001), Chinese Academy of Sciences (KGCX1-YW-13) and “863” project (2007AA100604 to Z.D.). The author gratefully acknowledges the support of K. C. Wong Education Foundation, Hong Kong (to F.S.). CryoEM data sets were collected at the National Resource for Automated Molecular Microscopy, which is supported by the National Institute of Health through the National Center for Research Resources' P41 program (RR17573).

Received: June 1, 2010

Revised: July 17, 2010

Accepted: July 27, 2010

Published: October 12, 2010

REFERENCES

Bigotti, M.G., and Clarke, A.R. (2008). Chaperonins: the hunt for the Group II mechanism. *Arch. Biochem. Biophys.* *474*, 331–339.

Booth, C.R., Meyer, A.S., Cong, Y., Topf, M., Sali, A., Ludtke, S.J., Chiu, W., and Frydman, J. (2008). Mechanism of lid closure in the eukaryotic chaperonin TRiC/CCT. *Nat. Struct. Mol. Biol.* *15*, 746–753.

Brunger, A.T. (2007). Version 1.2 of the Crystallography and NMR System. *Nat. Protoc.* *2*, 2728–2733.

Brunger, A.T., Adams, P.D., Clore, G.M., DeLano, W.L., Gros, P., Grosse-Kunstleve, R.W., Jiang, J.S., Kuszewski, J., Nilges, M., Pannu, N.S., et al. (1998). Crystallography & NMR System (CNS), A new software suite for macromolecular structure determination. *Acta Crystallogr. D Biol. Crystallogr.* *54*, 905–921.

Bukau, B., and Horwich, A.L. (1998). The Hsp70 and Hsp60 chaperone machines. *Cell* *92*, 351–366.

Carragher, B., Kisseberth, N., Kriegman, D., Milligan, R.A., Potter, C.S., Pulokas, J., and Reilein, A. (2000). Leginon: an automated system for acquisition of images from vitreous ice specimens. *J. Struct. Biol.* *132*, 33–45.

Clare, D.K., Stagg, S., Quispe, J., Farr, G.W., Horwich, A.L., and Saibil, H.R. (2008). Multiple states of a nucleotide-bound group 2 chaperonin. *Structure* *16*, 528–534.

DeLaBarre, B., and Brunger, A.T. (2006). Considerations for the refinement of low-resolution crystal structures. *Acta Crystallogr. D Biol. Crystallogr.* *62*, 923–932.

Emsley, P., and Cowtan, P.E.K. (2004). Coot: model-building tools for molecular graphics. *Acta Crystallogr.* *60*, 2126–2132.

Crowther, R.A., Henderson, R., and Smith, J.M. (1996). MRC image processing programs. *J. Struct. Biol.* *116*, 9–16.

DeLano, W.L. (2002). PyMOL Molecular Viewer. <http://www.pymol.org>.

Ditzel, L., Lowe, J., Stock, D., Stetter, K.O., Huber, H., Huber, R., and Steinbacher, S. (1998). Crystal structure of the thermosome, the archaeal chaperonin and homolog of CCT. *Cell* *93*, 125–138.

Esnouf, R.M. (1997). An extensively modified version of MolScript that includes greatly enhanced coloring capabilities. *J. Mol. Graph. Model.* *15*, 132–134.

Fernandez, J.J., Luque, D., Caston, J.R., and Carrascosa, J.L. (2008). Sharpening high resolution information in single particle electron cryomicroscopy. *J. Struct. Biol.* *164*, 170–175.

Frank, J., Radermacher, M., Penczek, P., Zhu, J., Li, Y., Ladjadj, M., and Leith, A. (1996). SPIDER and WEB: processing and visualization of images in 3D electron microscopy and related fields. *J. Struct. Biol.* *116*, 190–199.

Frydman, J., Nimmesgern, E., Erdjument-Bromage, H., Wall, J.S., Tempst, P., and Hartl, F.U. (1992). Function in protein folding of TRiC, a cytosolic ring complex containing TCP-1 and structurally related subunits. *EMBO J.* *11*, 4767–4778.

Gao, Y., Thomas, J.O., Chow, R.L., Lee, G.H., and Cowan, N.J. (1992). A cytoplasmic chaperonin that catalyzes beta-actin folding. *Cell* *69*, 1043–1050.

Goddard, T.D. (2007). Visualizing density maps with UCSF Chimera. *J. Struct. Biol.* *157*, 281–287.

Hemmingsen, S.M., Woolford, C., van der Vies, S.M., Tilly, K., Dennis, D.T., Georgopoulos, C.P., Hendrix, R.W., and Ellis, R.J. (1988). Homologous plant and bacterial proteins chaperone oligomeric protein assembly. *Nature* *333*, 330–334.

Iizuka, R., Yoshida, T., Shomura, Y., Miki, K., Maruyama, T., Odaka, M., and Yohda, M. (2003). ATP binding is critical for the conformational change from an open to closed state in archaeal group II chaperonin. *J. Biol. Chem.* *278*, 44959–44965.

Kim, S., Willison, K.R., and Horwich, A.L. (1994). Cytosolic chaperonin subunits have a conserved ATPase domain but diverged polypeptide-binding domains. *Trends Biochem. Sci.* *19*, 543–548.

Klumpp, M., Baumeister, W., and Essen, L.O. (1997). Structure of the substrate binding domain of the thermosome, an archaeal group II chaperonin. *Cell* *91*, 263–270.

Krissinel, E., and Henrick, K. (2007). Inference of macromolecular assemblies from crystalline state. *J. Mol. Biol.* *372*, 774–797.

Lander, G.C., Stagg, S.M., Voss, N.R., Cheng, A., Fellmann, D., Pulokas, J., Yoshioka, C., Irving, C., Mulder, A., Lau, P.W., et al. (2009). Appion: an integrated, database-driven pipeline to facilitate EM image processing. *J. Struct. Biol.* *166*, 95–102.

Lauerer, G., Kristjansson, J.K., Langworthy, T.A., and Stetter, K.O. (1986). *Methanothermus sociabilis* sp. Nov., a second species within the methanothermaceae growing at 97 °C. *Syst. Appl. Microbiol.* *8*, 100–105.

- Llorca, O., Smyth, M.G., Carrascosa, J.L., Willison, K.R., Radermacher, M., Steinbacher, S., and Valpuesta, J.M. (1999). 3D reconstruction of the ATP-bound form of CCT reveals the asymmetric folding conformation of a type II chaperonin. *Nat. Struct. Biol.* 6, 639–642.
- Ludtke, S.J., Baldwin, P.R., and Chiu, W. (1999). EMAN: semiautomated software for high-resolution single-particle reconstructions. *J. Struct. Biol.* 128, 82–97.
- McCoy, A.J., Grosse-Kunstleve, R.W., Adams, P.D., Winn, M.D., Storoni, L.C., and Read, R.J. (2007). Phaser crystallographic software. *J. Appl. Crystallogr.* 40, 658–674.
- Mindell, J.A., and Grigorieff, N. (2003). Accurate determination of local defocus and specimen tilt in electron microscopy. *J. Struct. Biol.* 142, 334–347.
- Morris, A.L., MacArthur, M.W., Hutchinson, E.G., and Thornton, J.M. (1992). Stereochemical quality of protein structure coordinates. *Proteins* 12, 345–364.
- Nitsch, M., Walz, J., Typke, D., Klumpp, M., Essen, L.O., and Baumeister, W. (1998). Group II chaperonin in an open conformation examined by electron tomography. *Nat. Struct. Biol.* 5, 855–857.
- Ochman, H., Gerber, A.S., and Hartl, D.L. (1988). Genetic applications of an inverse polymerase chain reaction. *Genetics* 120, 621–623.
- Otwinowski, Z.M., and Minor, W. (1997). Processing of X-ray diffraction data collected in oscillation mode. *Methods Enzymol.* 276, 307–326.
- Kraulis, P.J. (1991). MOLSCRIPT: a program to produce both detailed and schematic plots of protein structures. *J. Appl. Crystallogr.* 24, 946–950.
- Pettersen, E.F., Goddard, T.D., Huang, C.C., Couch, G.S., Greenblatt, D.M., Meng, E.C., and Ferrin, T.E. (2004). UCSF Chimera—a visualization system for exploratory research and analysis. *J. Comput. Chem.* 25, 1605–1612.
- Phipps, B.M., Hoffmann, A., Stetter, K.O., and Baumeister, W. (1991). A novel ATPase complex selectively accumulated upon heat shock is a major cellular component of thermophilic archaeobacteria. *EMBO J.* 10, 1711–1722.
- Powell, H.R. (1999). The Rossmann Fourier autoindexing algorithm in MOSFLM. *Acta Crystallogr. D Biol. Crystallogr.* 55, 1690–1695.
- Ranson, N.A., Clare, D.K., Farr, G.W., Houldershaw, D., Horwich, A.L., and Saibil, H.R. (2006). Allosteric signaling of ATP hydrolysis in GroEL-GroES complexes. *Nat. Struct. Mol. Biol.* 13, 147–152.
- Roseman, A.M. (2004). FindEM—a fast, efficient program for automatic selection of particles from electron micrographs. *J. Struct. Biol.* 145, 91–99.
- Schoehn, G., Quate-Randall, E., Jimenez, J.L., Joachimiak, A., and Saibil, H.R. (2000). Three conformations of an archaeal chaperonin, TF55 from *Sulfolobus shibatae*. *J. Mol. Biol.* 296, 813–819.
- Shaikh, T.R., Gao, H., Baxter, W.T., Asturias, F.J., Boisset, N., Leith, A., and Frank, J. (2008). SPIDER image processing for single-particle reconstruction of biological macromolecules from electron micrographs. *Nat. Protoc.* 3, 1941–1974.
- Shomura, Y., Yoshida, T., Iizuka, R., Maruyama, T., Yohda, M., and Miki, K. (2004). Crystal structures of the group II chaperonin from *Thermococcus* strain KS-1: steric hindrance by the substituted amino acid, and inter-subunit rearrangement between two crystal forms. *J. Mol. Biol.* 335, 1265–1278.
- Sousa, D., and Grigorieff, N. (2007). Ab initio resolution measurement for single particle structures. *J. Struct. Biol.* 157, 201–210.
- Suloway, C., Pulokas, J., Fellmann, D., Cheng, A., Guerra, F., Quispe, J., Stagg, S., Potter, C.S., and Carragher, B. (2005). Automated molecular microscopy: the new Legimon system. *J. Struct. Biol.* 151, 41–60.
- Tilly, K., Murialdo, H., and Georgopoulos, C. (1981). Identification of a second *Escherichia coli* groE gene whose product is necessary for bacteriophage morphogenesis. *Proc. Natl. Acad. Sci. USA* 78, 1629–1633.
- Wang, L., Hu, Z.J., Luo, Y.M., Huo, Y.W., Ma, Q., He, Y.Z., Zhang, Y.Y., Sun, F., and Dong, Z.Y. (2010). Distinct symmetry and limited peptide refolding activity of the thermosomes from the acidothermophilic archaea *Acidianus tengchongensis* S5(T). *Biochem. Biophys. Res. Commun.* 393, 228–234.
- Winn, M.D., Isupov, M.N., and Murshudov, G.N. (2001). Use of TLS parameters to model anisotropic displacements in macromolecular refinement. *Acta Crystallogr. D Biol. Crystallogr.* 57, 122–133.
- Wittig, I., Braun, H.P., and Schagger, H. (2006). Blue native PAGE. *Nat. Protoc.* 1, 418–428.
- Xu, Z., Horwich, A.L., and Sigler, P.B. (1997). The crystal structure of the asymmetric GroEL-GroES-(ADP)₇ chaperonin complex. *Nature* 388, 741–750.
- Yaffe, M.B., Farr, G.W., Miklos, D., Horwich, A.L., Sternlicht, M.L., and Sternlicht, H. (1992). TCP1 complex is a molecular chaperone in tubulin biogenesis. *Nature* 358, 245–248.
- Zhang, J., Baker, M.L., Schroder, G.F., Douglas, N.R., Reissmann, S., Jakana, J., Dougherty, M., Fu, C.J., Levitt, M., Ludtke, S.J., et al. (2010). Mechanism of folding chamber closure in a group II chaperonin. *Nature* 463, 379–383.